

# The Antarctic Dipole and its Predictability

Xiaojun Yuan and Douglas G. Martinson

Lamont-Doherty Earth Observatory, and Department of Earth and Environmental Sciences, Columbia University, Palisades, NY 10964

**Abstract.** This study investigates the nature of interannual variability of Antarctic sea ice and its relationship with the tropical climate. We find that the dominant interannual variance structure in the sea ice edge and surface air temperature fields is organized as a quasi-stationary wave which we call the “Antarctic Dipole” (ADP). It is characterized by an out-of-phase relationship between the ice and temperature anomalies in the central/eastern Pacific and Atlantic sectors of the Antarctic. The dipole consists of a strong standing mode and a weaker propagating motion within each basin’s ice field. It has the same wavelength as the Antarctic Circumpolar Wave (ACW) and dominates the ACW variance. The dipole is clearly associated with tropical ENSO events; it can be predicted with moderate skill using linear regression involving surface temperature two to four months ahead. The prediction performs better in extreme warm/cold years, and best in La Niña years.

## Introduction

The El Niño–Southern Oscillation (ENSO) signal has been identified in the Antarctic sea ice fields in many studies (*Chu, 1983; Carleton, 1989; Simmonds and Jacka, 1995; Ledley and Huang, 1997; Harangozo, 2000*). A more recent study found consistent (and statistically significant) teleconnection patterns linking Antarctic sea ice edge (SIE) variations to those of tropical and mid-latitude climate, as well as circumpolar variations amongst different polar basins (*Yuan and Martinson, 2000*). The strongest circumpolar teleconnection is characterized by a dipole-like pattern reflecting an out-of-phase relationship between Pacific and Atlantic polar regions, where the SIE is most responsive to extrapolar climate variability. This broad-scale covarying feature was called the Antarctic Dipole (ADP; *Yuan and Martinson, 2000*); it exists strongly in the surface air temperature (SAT) and SIE fields, and moderately in sea level pressure (SLP) fields. However, much of the interannual variability in the Southern Ocean has been described in the context of an Antarctic Circumpolar Wave (ACW) - a wavenumber two phenomenon propagating in ice, pressure, wind and temperature fields around the Antarctic (*White and Peterson, 1996*). The ACW has a period similar to the ENSO cycle. Consequently, we evaluate the variability of SIE, temperature and pressure fields in the context of standing versus propagating wave phenomena. Here we show that the ADP, a quasi-standing wave pattern, is the dominant interannual variability pattern in SIE and temperature. Moreover, we

establish linear regression models to predict the ADP using its relationship with lower latitude climate variability.

## Standing Wave versus Propagating Wave

We systematically examine the Antarctic dipole as manifested in the sea ice, temperature and pressure fields. Monthly surface air temperature and sea level pressure data from NCAR/NCEP reanalysis (*Kalnay et al., 1996*) were used. The SIE is derived from monthly sea ice concentration generated by the bootstrap algorithm from NASA microwave imager (*Comiso et al., 1997*). All data were low-pass filtered to remove sub-annual variability, and means were subtracted to yield anomaly fields, indicated by a prime. The first empirical orthogonal function (EOF) mode of  $SIE'$ , containing 37% of the total variance concentrated in the entire Western Hemisphere, clearly displays the ADP phenomenon (Figure 1a). Its poles are centered within the western Amundsen Sea and central Weddell Gyre. The temporal and spatial distribution of the  $SIE'$  leading mode emphasizes the dipole’s nature as a standing wave (Figure 1b). In addition to  $SIE'$ , it has been noted that SAT at weather stations display an out-of-phase relationship across the Antarctic Peninsula (*Comiso, 2000; Harangozo, 2000*). We conduct an EOF analysis on  $SAT'$  along  $65^{\circ}\text{S}$ , which reveals the same dipole pattern. The dipole in  $SAT'$  is best defined by the combination of the first two EOF modes (Figure 1c,d), containing 53% of the total variance.

To further explore the Antarctic Dipole expression in  $SAT'$  and  $SLP'$ , and identify its relationship with extrapolar climate, we conduct an EOF analysis on  $SAT'$  and  $SLP'$  in the Pacific and Atlantic, south of  $20^{\circ}\text{N}$ . The  $SAT'$  leading mode eigenvector (Figure 2a) shows a characteristic ENSO pattern with maximum amplitude centered in the central tropical Pacific. Associated with the tropical portion of this ENSO pattern is a circumpolar pattern that resembles the Antarctic Dipole in  $SIE'$ , showing a pole near  $60^{\circ}\text{S}$  in the South Pacific (of like-phase to the tropical signal) and another pole of opposite phase in the Weddell Gyre. This spatial pattern is very similar to the SST interannual variability pattern from Gurreaud and Battisti (*1999*). Moreover, a similar pattern is also found in the leading SVD mode for 30-years  $SAT'$  and sea ice concentration data (not shown here). However, the  $SLP'$  leading EOF mode does not display a profound dipole, but its dominant pattern is intriguing. The leading  $SLP'$  mode shows a zonal contrast between the eastern and central tropical Pacific reflecting the Southern Oscillation, as well as a striking meridional contrast between the tropical/mid-latitude and polar/subpolar regions in the Pacific. The meridional gradient is unevenly distributed in the Pacific and more evenly distributed in the Atlantic (Figure 2b). The correlation coefficient between

Copyright 2001 by the American Geophysical Union.

Paper number 2001GL012969.  
0094-8276/01/2001GL012969\$05.00

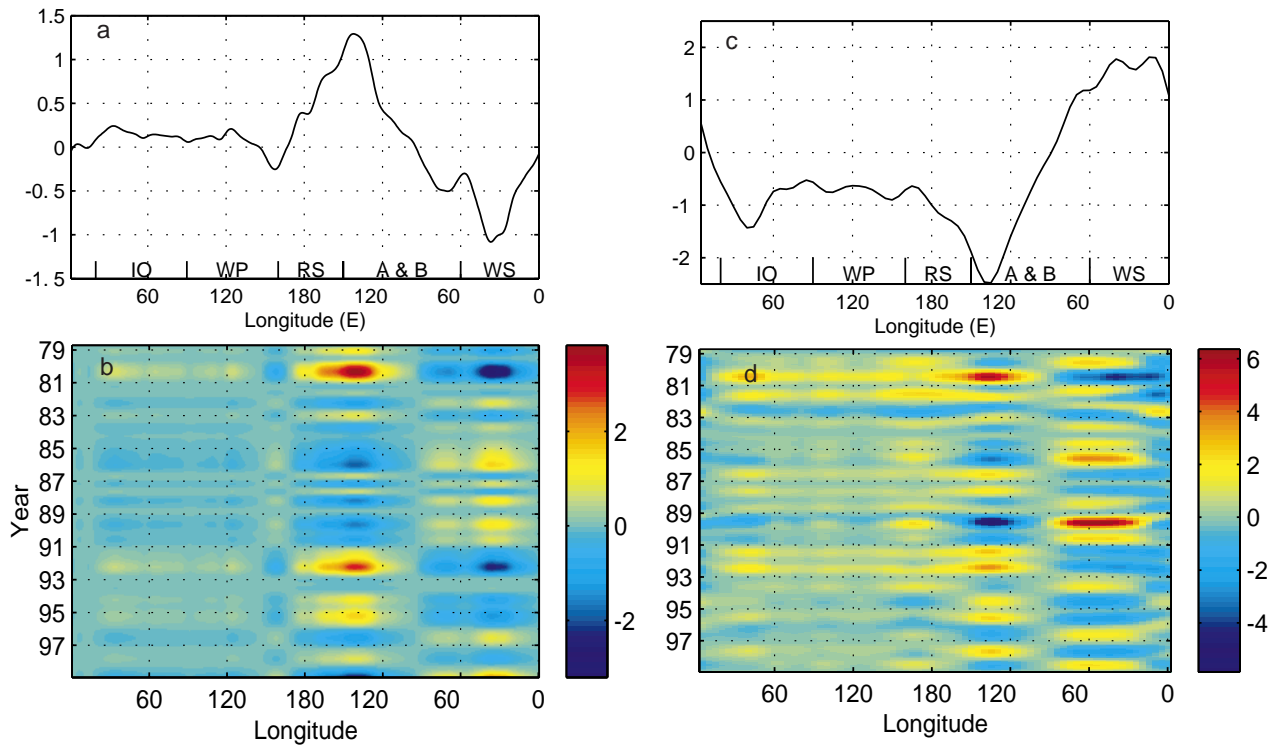


**Figure 1.** a: The eigenvector of the leading EOF mode of the  $SIE'$  (from 10/78 to 12/99) around the Antarctic (37% of the total variance). b: The  $SIE'$  containing only the first mode. c: Sum of eigenvectors from the first and second EOF modes of  $SAT'$  along  $65^\circ\text{S}$  containing 53% of the total variance. d: The  $SAT'$  along  $65^\circ\text{S}$  containing only first and second EOF modes. The Ross Sea, the Amundsen and Bellingshausen Sea, and the Weddell Sea are marked by RS, A&B and WS, respectively.

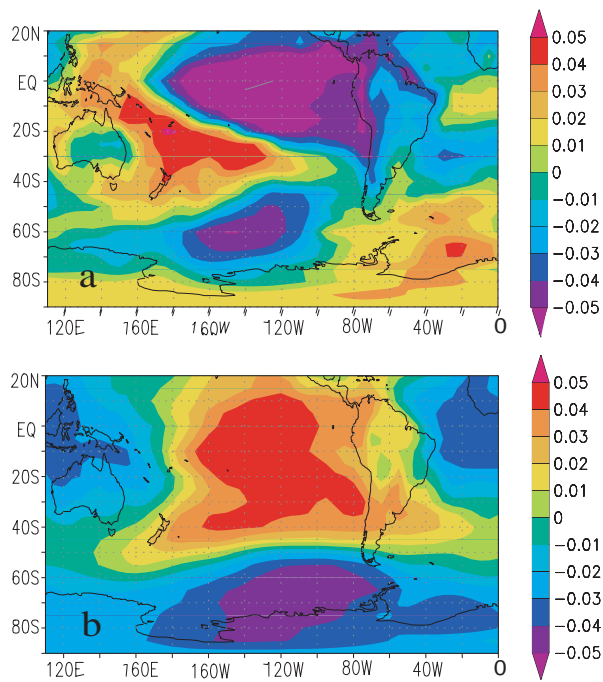


**Figure 2.** a: The leading EOF mode eigenvector of  $SAT'$  from 1975 to 1999 containing 18% of the total variance. b: The leading EOF mode eigenvector of  $SLP'$  containing 28% of the total variance in the same period as in figure 2a.

the time series (principal components: PCs) of  $SAT'$  and  $SLP'$  leading modes is 0.67 (significant at the 99% confidence level, accounting for temporal autocorrelations existing in both PCs).

Clearly, the Antarctic Dipole exists in both  $SIE'$  and  $SAT'$  fields. It is quite robust in both of the fields' total variance where it dominates the variability. Since it has approximately the same spatial wavelength as the ACW, it is necessary to differentiate these two phenomena. The leading mode of a complex EOF (CEOF) analysis (Wallace and Dickinson, 1972) applied to the  $SIE'$  field readily describes propagating motion (Figure 3a), consistent with an ACW. It shows that the strongest portion of the ACW signal is in the eastern Pacific and Weddell Gyre sectors of the Antarctic where the ADP exists. Outside of this region weaker signals appear that propagate at different speeds in different locations. The propagating signal consists of a strong static signal (the ADP) and a weaker propagating component as well. This is apparent by examining the real EOFs of the  $SIE'$  data. The first two modes are in quadrature, with the first mode representing a standing mode or, the dipole (Figure 1a,b). The second mode contributes an eastward propagation to the dipole, and together, the primary signal of the ACW in the  $SIE'$  becomes apparent. However, the propagation of the dipole signal appears to be contained within the individual basins (Figure 3b). This is also suggested by the total  $SIE'$  field (Figure 3c). Moreover, when we subtract the standing mode from the total  $SIE'$  field

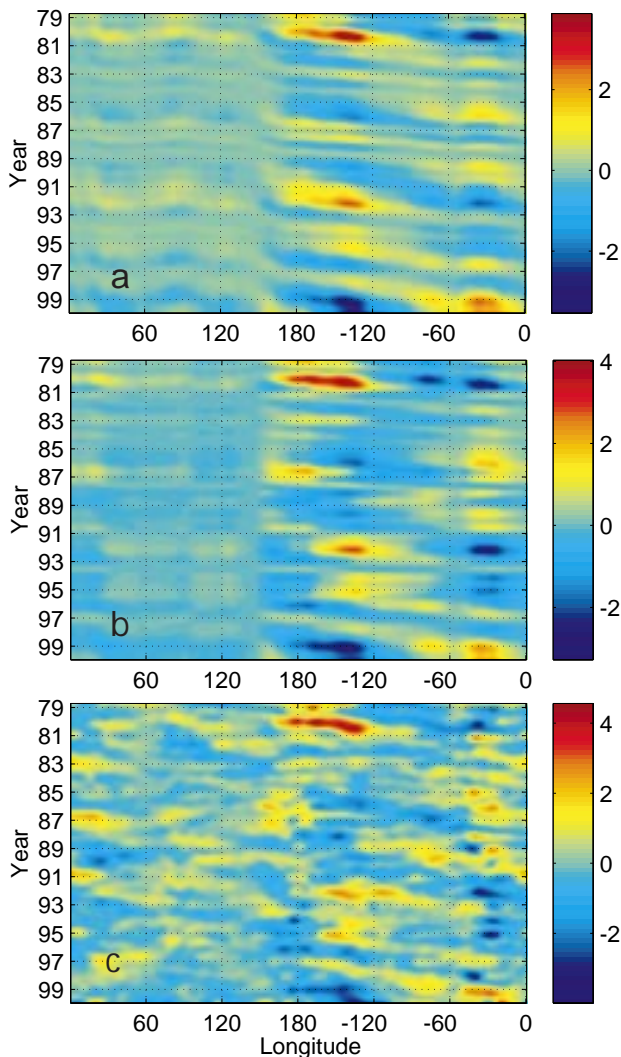


**Figure 3.** a: The  $SIE'$  containing only the first CEOF mode (40% of the total variance). b: The  $SIE'$  containing only first and second EOF modes (54% of total variance) as function of space and time. c: The  $SIE'$  as function of space and time.

and apply the CEOF analysis to the residual, we find the propagating signal becomes quite weak and is not consistently eastward. On the other hand, if we conduct a real EOF analysis on the CEOF leading mode (Figure 3a), the first mode is the ADP, which describes 83% of the total variance. The ADP, a standing mode with limited intra-basin eastward propagation, is the dominant mode of variability in the SIE field. A much weaker signal (approximately 20% or less of the total SIE variance) propagates outside of the dipole region. Since the ACW and ADP have approximately the same wavelength and similar period, they are likely related. Likely relationships include: (1) The ACW propagates through the area and excites the standing wave, and (2) the ADP is excited by extra-polar teleconnections and its anomaly is advected out of the dipole area by the Antarctic Circumpolar Current and/or air-sea-ice coupling processes. We favor the latter relationship for the following three reasons: (1) The eastern Pacific and Weddell Gyre regions are very sensitive to extra-polar climate (Peterson and White, 1998; Yuan and Martinson, 2000), (2) the ADP in  $SIE'$

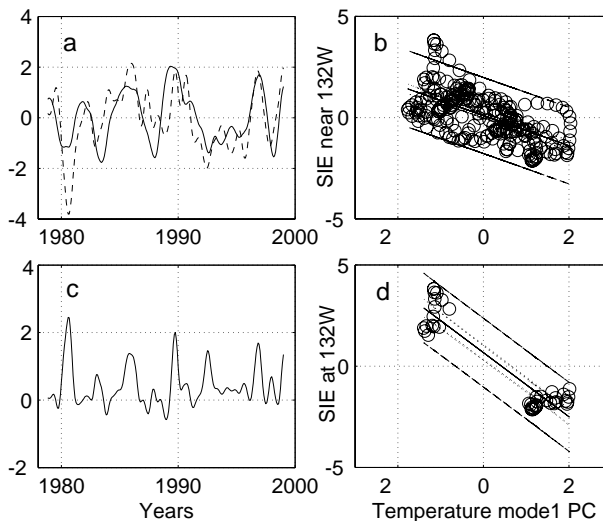


**Figure 4.** a: The SAT PC1 (dotted line) and the  $SIE'$  near  $132^\circ\text{W}$  as function of time ( $SIE'$  is lagged by four months). b: A scatter plot of the  $SIE'$  and SAT PC1 in a, and their linear regression. The 95% confidence levels for the regression line and for the individual point are marked. c: Instantaneous correlation coefficients between the two curves in panel a measuring the contribution at each time to the total correlation coefficient. d: Same as c except for points with instantaneous correlation above 1%.

can be predicted by extra-polar  $SAT'$  reasonably well during extreme cold and warm years (see next section) and (3) the magnitude of ADP variability is more than twice that of the ACW.

### Predictability of the ADP in SIE

The mechanisms responsible for the Antarctic Dipole and its link with extrapolar climate are not yet understood. We rely on the last two decades of satellite observations

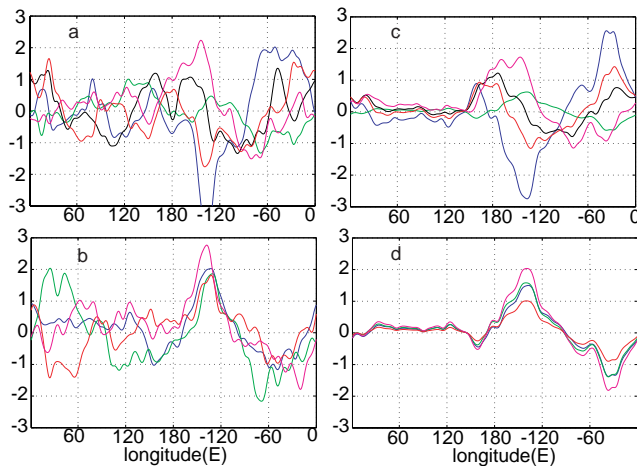


**Figure 5.** September (the maximum ice cover month in the Southern Hemisphere)  $SIE'$  as function of longitude following five EL Niño events in 1980, 1983, 1988, 1992 and 1997 (a) and four La Niña events in 1985, 1989, 1996 and 1999 (b). In the same way, September  $SIE'$  containing only the first EOF mode in the same El Niño years (c) and La Niña years (d).

and reanalysis products to statistically investigate the phenomenon. Figure 2 suggests that the Antarctic Dipole pattern is associated with interannual variability in the central tropical Pacific. We exploit this relationship to develop a linear prediction model whereby the leading mode PC of SAT (hereafter SAT-PC1) to forecast  $SIE'$  variations associated with the ADP.

The western Amundsen Sea SIE responds strongly to extrapolar climate variability while dominating the Pacific portion of the Antarctic Dipole oscillation (Figure 1). The correlation coefficient between the western Amundsen Sea  $SIE'$  and SAT-PC1 (the latter is leading by 4 months for the best correlation coefficient) is 0.62 at 99% confidence level (Figure 4a). All ice anomaly maxima correspond with the (five) maxima in SAT-PC1 representing cold (La Niña) central tropical Pacific anomalies. The ice responded well to the two warm events in the early 1980s and between 1992 and 1995, but failed to respond to the other three warm events (1983, 1988 and 1997). Figure 4b shows that a linear regression predict  $SIE'$  with large errors, the rms error is  $1^\circ$  of latitude. Examination of the correlation between western Amundsen Sea  $SIE'$  and SAT PC1 (Figure 4a) reveals that the largest contribution to the strong correlation between these two series occurs during extreme events. This suggests that extreme conditions in the tropics (especially cold conditions) likely trigger the large variations in the polar sea ice field. To test this, we calculated instantaneous correlations:

$$R_j = \frac{SIE'_j \times SAT'_j}{\sigma_{sie} \times \sigma_{sat} \times r} \quad j = 1, 2, \dots, 255$$

where  $\sigma$  is a standard deviation and  $r$  is the correlation coefficient between  $SIE'$  and  $SAT'$ . Clearly, the extreme events contribute more to the correlation than other times (Figure 4c). We then repeat the correlation and regression analysis by admitting only data points that contribute more than 1% to the overall correlation. This "threshold regression" reduces the rms error to 0.8 degree of latitude (Figure 4d). The correlation restricted to these supercritical values reaches 0.93. Therefore, we can hindcast extreme western Amundsen Sea ice conditions of the previous two decades quite well using temperature data four months in advance. In a similar manner, we can hindcast the ADP Index (defined by the difference between  $SIE'$  in the two dipole centers; near  $132^\circ\text{W}$  and  $24^\circ\text{E}$ ) using SAT-PC1 two months in advance. This linear regression explains 42% of the total variance. Again the hindcast is improved when we only consider the extreme cold and warm cases. This linear regression provides a prediction for ice conditions over a broader area than the previous one for the Western Amundsen Sea  $SIE'$ .

Finally, we examine how the maximum  $SIE'$  following ENSO events responds to the tropical forcing (Figure 5). The  $SIE'$  in the dipole region responds to the tropical conditions much more regularly than the SIE in other regions. Also apparent is the fact that the  $SIE'$  in the dipole regions responds more consistently to La Niña conditions than to El Niño conditions. The leading EOF mode of the  $SIE'$  strikingly demonstrates the later phenomenon. This is consistent with previous studies showing that the atmospheric circulation in the South Pacific failed to respond to ENSO warm events consistently (Karoly, 1989; Housego et al, 1998). The irregularity is likely caused by the varying evolution of

El Niño events in the absence of a single canonical evolution (Harangozo, 2000). Our study shows that  $SIE'$  more consistently respond to La Niña events than El Niño events. That makes the Antarctic Dipole most predictable during La Niña years.

**Acknowledgments.** Support for this research was provided by a NASA grant NAGS-8725 and an environmental research grant by Ford Motor Company. The sea ice concentration data were provided by NOAA's National Snow and Ice Data Center. Lamont-Doherty Earth Observatory contribution number 6189.

## References

- Carleton, A. M., Antarctic Sea-Ice Relationships with Indices of the Atmospheric Circulation of the Southern Hemisphere, *Climate Dynamics*, 3, 207-220, 1989.
- Chiu, L. S., Antarctic Sea Ice Variations 1973-1980, In: *Variations in the Global Water Budget*, Street-Perrot et al., eds., Reidel Publ., Dordrecht, 301-311, 1983.
- Comiso, J. C.: Variability and Trends in Antarctic Surface Temperatures from In Situ and Satellite Infrared Measurements. *J. Clim.*, 13, 1674-1696, 2000.
- Comiso, J. C., D. J. Cavalieri, C. L. Parakinson and P. Gloersen, Passive Microwave Algorithms for Sea Ice Concentration: A Comparison of Two Techniques. *Remote Sens. Environ.*, 60, 357-387, 1997.
- Garreaud, R. D. and D. S. Battisti, Interannual (ENSO) and Interdecadal (ENSO-like) Variability in the Southern Hemisphere Tropospheric Circulation. *J. Climate*, 12, 21113-2123, 1999.
- Harangozo, S.A.: A search for the ENSO teleconnections in the west Antarctic Peninsula climate in austral winter. *Int. J. Clim.*, 20, 663-679, 2000.
- Housego, R., G. McGregor, J.C. King and S.A. Harangozo: Climate Anomaly Wave-train Patterns Linking Southern Low and High Latitudes During South Pacific Warm and Cold Events. *Int. J. Climatol.*, 18, 1181-1193, 1998.
- Ledley, T. S. and Z. Huang, A Possible ENSO signal in the Ross Sea, *Geophys. Res. Lett.*, 24, 3253-3256, 1997.
- Kalnay E. et al. The NCEP/NCAR 40-year reanalysis project. *Bulletin of the American Meteorological Society*, 1996.
- Peterson, R. G. and W. B. White: Slow teleconnections linking the Antarctic Circumpolar Wave with the tropical El Niño-Southern Oscillation. *J. Geophys. Res.*, 103, 24573-24583, 1998.
- Simmonds, I. and T. H. Jacka, Relationships between the Interannual Variability of Antarctic Sea Ice and the Southern Oscillation, *J. Climate*, 8, 637-647, 1995.
- Wallace, J. M. and R. E. Dickinson: Empirical Orthogonal Representation of time series in the frequency domain. Part I: Theoretical Considerations. *Journal of Applied Meteorology*, 11, 887-900, 1972.
- White, B. W. and R. G. Peterson: An Antarctic circumpolar wave in surface pressure, wind, temperature and sea ice extent. *Nature*, 380, 699-702, 1996.
- Trenberth, K. and T.J. Hoar: The 190-1995 El N/ noSouthern Oscillation. *Geophys. Res. Letter*, 23, 57-69, 1996.
- Yuan, X. and D. G. Martinson, Antarctic Sea Ice Extent Variability and its Global Connectivity, *J. of Climate*, 13, 1697-1717, 2000.

X. Yuan and D.G. Martinson, Lamont-Doherty Earth Observatory, and Department of Earth and Environmental Sciences, Columbia University, Palisades, NY 10964

(Received February 5, 2001; revised April 23, 2001; accepted April 30, 2001.)